The 2013 World Congress on
Advances in Structural Engineering and Mechanics (ASEM13)
Jeju, Korea, September 8-12, 2013

Post failure localization instabilities in chemically active creeping faults: Steady-state bifurcation and transient analysis

*Sotirios Alevizos[1)], Emmanuil Veveakis[2)] and Yannis F. Dafalias[3)]

[1),3)] *Dept. of Applied Mathematics and Physics, National Technical Univ. of Athens, Zographou, 15773 Athens, Greece*
[2)] *CSIRO Earth Science and Resource Engineering, ARRC, 26 Dick Perry Avenue, Kensington WA, 5151*
[1)] *sotiris@mechan.ntua.gr*

ABSTRACT

In this paper we emphasize in the post failure evolution of a creeping fault, and provide temporal and spatial modes of evolution. In particular we study the behavior of a fluid-saturated fault under shear, based on the assumption that the fabric presents rate- and temperature dependent response to shear loading. A creeping fault of this type can, under certain conditions produce excess heat due to shear heating, reaching temperatures which are high enough for triggering endothermic chemical reactions. We focus on the decomposition reactions and incorporate excess pore pressure generation and variations of the porosity due to the chemical effects (a process called chemical pressurization). After deriving the corresponding system of equations in the region of the ultra-cataclastic core, we study the influence of the model parameters, namely the frictional, hydraulic and chemical properties of the material, along with the boundary conditions of the problem, on the behavior of the fault and through a non-linear bifurcation analysis we provide regimes of stable-frictional sliding and pressurization. Furthermore, the system is integrated in time to extract its temporal behavior, providing regimes of stable creep, non-periodic and periodic seismic slip events due to chemical pressurization, depending on their frictional properties. It is shown that this chemically induced seismic slip is an ultra-localized event in the post failure regime. It takes place in an extremely narrow band, 2 orders of magnitude narrower than the initial one, verifying the field observations.

1. INTRODUCTION

Field observations of faults that have experienced a large slip, show a generally broad zone of damaged rock, but nevertheless suggest that shear localization occurs in very narrow zones of few millimeters to centimeters thick, at most (Rice 2006). As

[1)] Ph.D.
[2)] Ph.D.
[3)] Professor

these fault slip zones are very thin, thermal effects during rapid slip may be of primary importance. Indeed, coupled effects including shear heating and pore fluid pressurization are considered to be the primary weakening mechanisms during fault slip (Rice 2006) or catastrophic landslides (Vardoulakis 2002). Recently, thermo-poro-mechanical couplings due to shear heating are being considered the cause of inducing chemical effects in faults such as dehydration of minerals and decomposition of carbonates, theoretically studied in Brantut et al. (2008, 2010), Sulem and Famin (2009) and reported to take place in real faults (Famin et al. 2008, Hirono and et al. 2007) or at laboratory conditions (Han et al. 2007, Ferri et al. 2010).

In our previous work (Veveakis et al. 2010) we have showed that in modeling of such behaviors (such as faults experiencing prolonged slip) that span in more than one timescale, we commonly account for rate and state dependency in the frictional behavior of the geomaterials, after the works of Dieterich (1972, 1978) and Ruina (1983). We depicted that all the commonly assumed friction laws provide the same steady-state response up to the onset of an instability, where dissipation localizes in the vicinity of the fault's core. Upon reaching this state, temperature increases high enough to trigger the endothermic chemical reaction with the smaller activation temperature at the considered pressure state. Past this point, the behavior of the fault is determined by the characteristics of the chemical reaction triggered, usually causing dynamic drop on the fault's strength in the form of excess pore fluid generation or lubrication.

Indeed, when applied to clays, these models lead to the triggering of thermal pressurization after long, stable slip where shear heating was producing heat due to friction (Veveakis et al. 2007). Recently, it has been reported experimentally (Ferri et al. 2010) and studied theoretically (Brantut et al. 2010) the fact that instead of thermal pressurization, chemical pressurization caused by a decomposition reaction may produce fluid leading to the reduction of the fault's strength. In addition, amorphization reactions (Yund et al. 1990, Brantut et al. 2008) like melting may also reduce rapidly the strength of a fault in the absence of pore fluid generation. Since all these weakening processes are thermal in origin (Rice 2006), it is anticipated that triggering one of them could be due to the heat produced by friction at the base of a slipping fault.

In this study we extend the results of Veveakis et al. (2010) by considering the presence of a decomposition reaction for the fault's minerals (Veveakis et al. 2012). Based on the principles of thermodynamics and reaction kinetics we formulate the corresponding governing equations and constitutive laws for the problem of simple shear of a biphasic granular material. Following our previous findings, we introduce power-law rate- and Arrhenius-type thermal- dependency on the friction law. We apply the model to the specific reaction of calcite decomposition (Sulem and Famin 2009), which is reported to take place in real faults and influences the fault's friction (Han et al. 2007), by producing CO_2 at supercritical, fluid phase and provide results on the steady state and transient behavior of the system.

2. PROBLEM FORMULATION

In order to model such effects, we consider a porous medium consisting of a solid AB, being fully saturated with a fluid B. We use indexes or superscripts s and f for

denoting a field for solid and fluid phase, respectively. At high temperatures the solid phase decomposes, following a reaction of the form:

$$AB \leftrightarrow A + B \tag{1}$$

We assume that the reaction rate of this reaction follows the Arrhenius law, $\omega \propto e^{-E/RT}$, where k is the pre-exponential factor of the reaction (in s^{-1}) and E its activation energy, (Sulem and Famin 2009). In principle both k and E could be temperature, pressure and grain-size dependent, as discussed in Veveakis et al. (2012), however the absence of valid experimental data at temperature and pressures met in real faults restricts us to assume them constant.

In the following we briefly present the governing equations of the specific problem at hand, along with the appropriate constitutive laws for the various processes involved. We focus in the problem of a fault under shear, consisting of a fully saturated in fluid B soil skeleton, and deforming under constant volume (zero volumetric strain rate). We model the fault as an infinite shear zone of thickness d inside a large rock mass (Fig. 1), thus allowing for the various fields involved to vary only in time and in the z-direction. We assume that the material has undergone all the elastic deformations at the initial stage of its response, contributing to form an initial, thermoplastic configuration (Rice 2006).

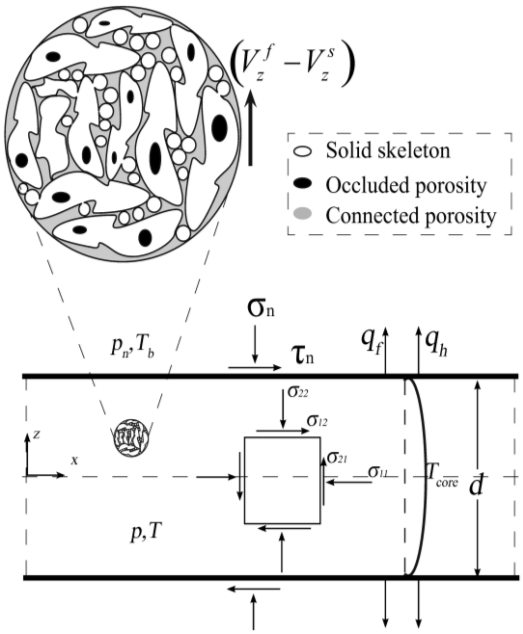

Fig. 1 Problem formulation. The loading conditions and the filter velocity $v_z^f - v_z^s$, along the content of a biphasic mixture, are depicted. Notice that, in the absence of experimental data at the grain scale, we assume that the chemical reaction is taking place at the grain-pore interface. Hence, all the produced fluid contributes to the interconnected pore volume and is concentrated on the grain boundaries. In addition, we assume that the produced solid is incorporated to the skeleton, establishing a common velocity field v_z^s with the reactant solid.

2.1 Stress Equilibrium

It is commonly assumed in the literature (Rice 2006, Sulem and Famin 2009) that due to the small thickness of the shear band, inertia terms may be neglected, leading to uniform in space, constant across the shear band, stress fields. Thus, $\sigma_{zz} = \sigma_n(t)$ and $\tau = \tau_n(t)$ are the normal and shear stresses acting in the shear band. The normal stress is assumed to obey Terzaghi's principle, $\sigma_{zz} = \sigma'_{zz} + p$ (stresses are taken negative at compression) - the prime denoting effective stress (i.e. σ'_{zz} is the normal effective stress at z-direction) – where $p = p_n + \Delta p$, p_n being the hydrostatic pressure at the boundary and Δp the excess pore pressure. Since inside the shear band normal stress is constant across it and equal to its value at the boundary $\sigma_{zz} = \sigma_n(t)$, then $\sigma'_{zz} = \sigma'_n + \Delta p$. By using Coulomb's law, we then obtain $\tau = \mu(\dot{\gamma}, T)\sigma'_{zz}$, where $\mu(\dot{\gamma}, T)$ is the friction coefficient, assumed here a function of the strain-rate and temperature, after the results of Veveakis et al. (2010).

2.2 Mass Considerations

Even though the total mass of the mixture remains constant, this is not true for each of the constituents. The rate of mass variations of each of them is a function of the reaction rates of the forward and reverse reaction, $\omega_F = (\rho_1/M_{AB})k_F\, e^{-E_F/RT}$ and $\omega_R = \left(\rho_2\rho_f/M_A M_B\right)k_R\, e^{-E_R/RT}$. In these expressions we denote with k_F, k_R, E_F, E_R the pre-exponential factors and activation energies of the forward and reverse reaction, respectively, M_i the molar mass of the i−th constituent and $\rho_1 = (1-\varphi)(1-s)\rho_{AB}$, $\rho_2 = (1-\varphi)s\rho_A$, $\rho_s = \rho_1 + \rho_2$, $\rho_f = \varphi\rho_B$ the partial densities of AB, A, the solid's phase consisting of both AB and A, and fluid's phase consisting of B (pre-existing and chemically produced), respectively. These partial densities are defined through the porosity, φ, and the partial solid ratio (the ratio of the produced solid A), s,

$$\varphi = \varphi_0 + \Delta\varphi = \frac{V_B}{V}, s = \frac{V_B}{V_s} = \frac{V_B}{(1-\varphi)V} \tag{2}$$

where φ_0 is the initial (mechanical) porosity - constant under the assumption of critical state – and $\Delta\varphi$ the new interconnected pore volume created from the reaction, which - along with s - is calculated directly from the reaction's characteristics, to be

$$\begin{gathered}\Delta\varphi = A_\varphi(1-\varphi_0)\left(1+\frac{\rho_B}{\rho_A}\frac{M_A}{M_B}\frac{k_F}{k_R}\frac{1}{s}\right)^{-1} \approx (1-\varphi_0)\left(1+\frac{\rho_B}{\rho_A}\frac{M_A}{M_B}\frac{1}{s}\right)^{-1} \\ s = \frac{\omega_{rel}}{1+\omega_{rel}} \\ \omega_{rel} = \frac{\rho_{AB}}{\rho_A}\frac{M_A}{M_{AB}}K_c e^{-\Delta E/RT}\end{gathered} \tag{3}$$

In Eqs. (3), $K_c = k_F/k_R$ is the ratio of the pre-exponential factors of the Arrhenius reaction rates (forward over reverse reaction) and $\Delta E = E_F - E_R$ the difference of the forward and reverse activation energies. The parameter A_φ is a coefficient that determines the amount of the interconnected pore-volume (porosity) created due to the reaction. In the absence of any other information from the micromechanics of chemical reactions in porous media, we assume that all the fluid created contributes to the

interconnected pore volume and thus set $A_\varphi = 1$ in Eq. (3). The model of Eqs. (3) can be calibrated for a specific reaction – in Table 1 (section 3) we present the corresponding values for calcite decomposition.

We assume that the fluid B is compressible obeying the standard equation of state $d\rho_B/\rho_B = \beta_f dp - \lambda_f dT$, where β_f and λ_f the fluid's compressibility and thermal expansion coefficient, respectively. For incompressible solids AB and A, mass balance equations could be derived for each one of the phases,

$$\frac{\partial \rho_s}{\partial t} + \frac{\partial \rho_s v_z^s}{\partial z} = j_s$$
$$\frac{\partial \rho_f}{\partial t} + \frac{\partial \rho_f v_z^f}{\partial z} = j_f \tag{4}$$

where $j_s = \omega_{AB} M_{AB} + \omega_A M_A < 0$ and $j_f = \omega_B M_B > 0$. In order for the total mass to be conserved $j_f = -j_s$. In Eqs. (4) v_i^α denotes the i-th component of the velocity (i = x, z) of the two phases (α = s, f), namely the solid skeleton (consisting of AB and A) and fluid B. In Soil Mechanics literature, these mass fluxes are usually related to the pore pressure gradient through Darcy's law, expressed for Gersevanov's filter velocity $\varphi\left(v_z^f - v_z^s\right)$ (Vardoulakis and Sulem 1995),

$$q_f = \varphi\left(v_z^f - v_z^s\right) = -\frac{k_\pi}{\mu_f}\frac{\partial \Delta p}{\partial z} \tag{5}$$

where μ_f is the viscosity of the fluid in $Pa \cdot s$, k_π the permeability and Δp the excess pore-pressure. Concerning the permeability, we rely on Kozeny-Carman's relationship:

$$k_\pi = k_{\pi 0} \frac{(1-\varphi_0)^2}{{\varphi_0}^3} \frac{\varphi^3}{(1-\varphi)^2} \tag{6}$$

$k_{\pi 0}$ being a reference permeability at porosity φ_0 (Sulem and Famin 2009).

2.3 Energy Considerations

The energy balance law, combined with the second law of thermodynamics, Fourier's law of isotropic conduction and by neglecting any thermoelastic heating effects, yields the heat equation (Veveakis et al. 2010)

$$\frac{D^{(m)}T}{Dt} = \kappa_m \frac{\partial^2 T}{\partial x_k^2} + \frac{\delta_{loc}}{(\rho C)_m} \pm \frac{|\Delta H|\omega_F}{(\rho C)_m} \tag{7}$$

where ΔH is the reaction's specific enthalpy, $\kappa_m = k_m/(\rho C)_m$ is Kelvin's thermal diffusion coefficient of the mixture, $k_m = (1-\varphi)k_s + \varphi k_f$ is the thermal conductivity of the soil-water mixture and k_s, k_f are Fourier's thermal conductivities of the solid and fluid, respectively. Also, $C_m = -T\,\partial^2\psi/\partial^2 T$ is the specific heat capacity of the mixture. The latter is calculated in reference to the partial masses of the constituents, through

mixture's theory, $(\rho C)_m = (1-\varphi)\rho_s C_s + \varphi\rho_f C_f$, where C_s and C_f is the specific heat of the solids and of the fluid, respectively. In the derived heat diffusion equation for a biphasic mixture under constant volume (Eq. 7) the second r.h.s term is the deformal power that is converted into heat, i.e.

$$\delta_{loc} = \beta_T \sigma \dot{\epsilon}^p \tag{8}$$

where the Taylor-Quinney ratio β_T expresses the amount of the mechanical energy converted into heat, and is in principal a history dependent quantity, rather than a constant ($0 \leq \beta_T \leq 1$). In this study this ratio cannot be a priori determined, since there are numerous processes in the grain-to-grain scale (eg. wear, breakage, intergranular rolling, flash heating etc.) that should be individually characterized concerning their influence on the dissipation function. Thus, throughout this study β_T will be treated as a free parameter in order to depict its influence on the stability of the system, relegating all its rate and state dependencies in the expression of δ_{loc}, through the well-established constitutive model of rate-and-state dependency of the friction coefficient.

2.4 Constitutive modeling of rate and thermal dependent plasticity

In this work we emphasize in the case of an active, preexisting fault. Thus we study the post failure regime, acknowledging the role of elasticity influencing the initial configuration of the present model (Rice 2006). Under this assumption, during simple shear, the failure (cohesionless Mohr-Coulomb) criterion is assumed to be met, providing for the yield shear stress τ_n,

$$\tau_n = \mu(\dot{\gamma}, T)\sigma'_{zz} \tag{9}$$

where $\mu(\dot{\gamma}, T)$ is the friction coefficient, incorporating the thermal and (plastic) rate dependency of the Taylor-Quinney coefficient β_T.

The role of temperature in failure of soft geomaterials is an open field of research in the area of geomechanics, mainly due to the vast interest in nuclear waste disposal problems. In this study, the thermal signature of the shear process could reflect all the micromechanical mechanisms -like mylonization, brecciation, asperities of rock-to-rock or harder materials' contacts- taking place at the microstructure of the sheared fault zone, increasing (harden) or decreasing (weaken) its frictional response and changing its (average) temperature. By implicitly linking the micro-processes to the average temperature of the fault, we have to assume that the thermal contribution will be acting antagonistically with respect to the rate dependency, so that the friction coefficient is able to admit a constant value, as required by the critical state theory of geomaterials. Hence, thermal softening is accompanied by rate (velocity) hardening (Velocity-Hardening/Thermal-Softening case, hereafter called VHTS) and vice versa (Velocity-Softening/Thermal- Hardening response, hereafter called VSTH).

As it was shown recently by Veveakis et al. (2010), the most commonly used rate and temperature dependent friction laws would provide similar results, with the one admitting power-law rate- and Arrhenius-type thermal- dependency being the most general and physically meaningful one. Thus, for the problem of simple shear we multiplicatively decompose the friction coefficient of Eq. (9) into a thermal and a strain

rate dependent part, in order to be able to obtain constant friction coefficients (as in critical state):

$$\mu(\dot{\gamma},T)=\mu_0 f(\dot{\gamma})g(T), f(\dot{\gamma})=\left(\frac{\dot{\gamma}}{\dot{\gamma}_0}\right)^N, g(T)=e^{\frac{T_d}{T}} \tag{10}$$

where μ_0 and $\dot{\gamma}_0$ reference quantities for the friction coefficient and the strain rate, whereas $T_d=E_d/R$ and N the thermal and rate sensitivities of friction, respectively. Following Veveakis et al. (2010) we require $0<|N|<1$ so that the shearing resistance remains bounded and set $E_d=xE_F$, i.e. that the activation energy of the friction process is a portion x of the activation energy of the chemical reaction to facilitate the mathematical formulation. Although x could in principle be larger than N, we restrict our study to more realistic values of the ratio $x/N<1$, as shown in Veveakis et al. (2010). Notice that x and N have always the same sign on this study, in order to assure that thermal and rate sensitivity are acting antagonistically.

Based on the findings of Section 2.1, $\tau_n=\mu(\dot{\gamma},T)\sigma'_{zz}=\mu(\dot{\gamma},T)[\sigma'_n-\Delta p(t)]$, or

$$\tau_n=\mu_0\sigma'_n\left(\frac{\dot{\gamma}}{\dot{\gamma}_0}\right)^N e^{\frac{E_d}{RT}}\left(1-\frac{\Delta p}{\sigma'_n}\right) \tag{11}$$

We will restrict this study in creep phenomena, where a fault deforms under constant (in time) applied normal and shear load, $\sigma'_n=const.$ and $\tau_n=const.$ Hence, from Eq. (11) we may invert for the strain-rate, to obtain

$$\dot{\gamma}=\dot{\gamma}_0\left(1-\frac{\Delta p}{\sigma'_n}\right)^{-1/N} e^{-\frac{E_d}{NRT}} \tag{12}$$

Since the dissipation due to the skeleton's shear component is significantly larger that both the skeleton's volumetric and the fluid dissipation, the deformal power converted into heat, Eq. (8), reduces into the following expression:

$$\delta_{loc}=\beta_T\tau_n\dot{\gamma}=\beta_T\tau_n\dot{\gamma}_0\left(1-\frac{\Delta p}{\sigma'_n}\right)^{-1/N} e^{-\frac{E_d}{NRT}} \tag{13}$$

2.5 Summary of the Equations

The final set of equations consists of the mass balance equations, Eqs. (4), the heat equation (7), as well as the constitutive relations, Eqs. (3), (5), (6) and (9). Following the above considerations, we obtain the final system of equations, Eqs. (14), where $\rho_s=\rho_1+\rho_2$, $\omega_F=(1-\varphi)(1-s)(\rho_{AB}/M_{AB})k_F\, e^{-E_F/RT}$ and $D^{(\alpha)}/Dt=\partial/\partial t+v_z^{\alpha}\,\partial/\partial z$ is the material time derivative.

$$\begin{gathered}\frac{D^{(s)}\rho_s}{Dt}+\rho_s\frac{\partial v_z^s}{\partial z}=-M_B\omega_F\\ \beta_f\frac{D^{(s)}\Delta p}{Dt}-\lambda_f\frac{D^{(s)}T}{Dt}+\frac{1}{\varphi}\frac{D^{(s)}\varphi}{Dt}+\frac{q_f}{\varphi}\left(\beta_f\frac{\partial\Delta p}{\partial z}-\lambda_f\frac{\partial T}{\partial z}\right)+\frac{\partial v_z^s}{\partial z}=-\frac{1}{\varphi}\frac{\partial q_f}{\partial z}+\frac{M_B}{\rho_f}\omega_F\\ (\rho C)_m\frac{D^{(m)}T}{Dt}=k_m\frac{\partial^2 T}{\partial z^2}+\beta_T\tau_n\dot{\gamma}_0\left(1-\frac{\Delta p}{\sigma'_n}\right)^{-1/N} e^{-\frac{E_d}{NRT}}-|\Delta H|\omega_F\end{gathered} \tag{14}$$

3. REDUCTION OF THE SYSTEM AND PARAMETRIC ANALYSIS

3.1 Reduction of the system

We may bring the system of the governing equations into a dimensionless form, by introducing the quantities

$$t^* = \frac{\kappa_m}{(d/2)^2} t, z^* = \frac{z}{d/2}, T^* = m(T - T_c), \Delta p^* = \frac{\Delta p}{\sigma_n'} \tag{15}$$

where T_c is a reference temperature, usually identified either as a reference temperature at which material properties are determined, as the maximum temperature that the process may admit or as the boundary temperature. In this study we accept the former (reference temperature where the material properties are determined), so that the effect of the boundary conditions on the stability of the system can also be studied. In the present work, drained-isothermal conditions ($\Delta p_{bound} = 0$ and $T_{bound} = T_b$) for the shear-band boundary will be combined with the standard symmetry conditions $\partial T/\partial z = \partial \Delta p/\partial z = 0$ at the center of the shear band (Chen et al. 1989).

By assuming that the convective terms in the mass balance equations are negligible, which is expected to hold true for relatively shallow faults, the final system of equations take the form (the superimposed asterisks are dropped for convenience)

$$\begin{aligned} \frac{\partial \Delta p}{\partial t} &= \frac{1}{Le}\frac{\partial^2 \Delta p}{\partial z^2} + \zeta \mu_r e^{\frac{Ar\delta T}{1+\delta T}} \\ \frac{\partial T}{\partial t} &= \frac{\partial^2 T}{\partial z^2} + \left[Gr(1-\Delta p)^{-1/N} e^{\frac{\alpha Ar}{1+\delta T}} - 1\right] e^{\frac{Ar\delta T}{1+\delta T}} \end{aligned} \tag{16}$$

where the assumption $(1 - \varphi_0) \approx 1$ was also made, due to $\varphi_0 \ll 1$.

The dimensionless groups appearing in the system (21) are defined as

$$\begin{aligned} Le = \frac{\kappa_m \mu_f}{k_\pi \sigma_n'}, \mu_r = \frac{(d/2)^2}{\kappa_m \sigma_n'}\frac{k_F}{\beta_f} e^{-Ar}, Ar = \frac{E_F}{RT_c} \\ \alpha = 1 - \frac{x}{N}, x = \frac{E_d}{E_F}, \delta = \frac{1}{mT_c}, m = \frac{k_m}{|\Delta H|(d/2)^2}\frac{e^{Ar}}{k_F \rho_{AB}} \\ Gr = \frac{\beta_T \tau_n \dot{\gamma}_0}{|\Delta H| k_F \rho_{AB}}, \zeta = \frac{\rho_m}{\rho_B}\frac{M_B}{M_{AB}}(1 - \varphi_0) \end{aligned} \tag{17}$$

The system of Eqs. (16) is valid for settings near its steady state the constitutive assumptions of these problems are valid only in the vicinity of steady state conditions. This is true for Darcy's law of hydraulic diffusion, Fourier's law of conduction, the Arrhenius law of kinetics, but also the rate and state dependence of friction, which is a valid concept only when considering slips that are large enough, and have the velocity changing slowly, so that the friction coefficient can be equated to its steady state value at rate $\dot{\gamma}$ (Rice 2006). Thus, by accepting the above we restrict the model to deformations that can always be tracked back to a steady state condition, where the convective terms appearing in the heat equation are negligible, since the integration of the mass balance of the mixture at steady state, along with continuity of the velocity fields across the shear-zone yield $v_z^m = 0$. In this study, the thermal convective terms

(convective terms appearing in temperature diffusion equation) are zero at steady-state, whereas in the transient problem they are negligible as long as they are of lower order than the leading terms. This is true when

$$k_{\pi 0} < k_m \frac{\mu_f}{|\Delta H| k_F \rho_{AB}} \frac{e^{Ar}}{\sigma_n'} \tag{18}$$

For the reference values of Table 1, this condition yields $k_{\pi 0}\sigma_n' < 10^{-17}\ [m^2 MPa]$, thus the deeper the fault the more important the convective terms are, in agreement with Rognon and Einav (2010).

3.2 Parametric Analysis

The behavior of the system is evidently characterized by the set of dimensionless parameters appearing in Eqs. (16). Prior to studying their effect on the system's response we need to understand the physical importance of each one and identify those varying the most so that they be used as bifurcating parameters.

Table 1. Indicative material parameters for a fault at $7km$ depth. We accept $E_F = |\Delta H|$ and $\beta_f \approx 10^{-3} MPa^{-1}$, $\lambda_f \approx 10^{-3}$ ℃$^{-1}$ and $N = 0.1$ in creep deformation. For these values of the parameters and for $T_c = 600$℃ the corresponding dimensionless groups are $Ar = 40$, $\delta = 0.0026$, $\mu_r = 0.003$, $Le \approx 0.7$ for $k_{\pi 0} = 10^{-17} m^2$. Since however the value permeability may vary significantly (from $10^{-15} m^2$ to $10^{-21} m^2$), it is rational to assume that the Lewis number lies between 10^{-3} to 10^3, being around 1 for $k_{\pi 0} = 10^{-18} m^2$ and $\varphi = \varphi_0$. The value of boundary temperature follows the geothermal gradient ($T_b = 210$℃ at $7km$ depth) and we assume that the fault is not in a pressurized aquifer, $\Delta p_b = 0$.

Parameter	Value	Units
$\boldsymbol{\varphi_0}$	0.03	–
$\boldsymbol{k_m}$	10^{-1}	$J/(Cms)$
$\boldsymbol{\sigma_n'}$	120	MPa
$\boldsymbol{d}$	10^{-3}	m
$\boldsymbol{M_{CaCO_3}}$	0.1	kg/mol
$\boldsymbol{\kappa_m}$	10^{-6}	m^2/s
$\boldsymbol{M_{CaO}}$	0.056	kg/mol
$\boldsymbol{k_{\pi 0}}$	10^{-21}– 10^{-15}	m^2
$\boldsymbol{M_{CO_2}}$	0.044	kg/mol
$\boldsymbol{k_F}$	10^15	$1/s$
$\boldsymbol{\rho_{CaCO_3}}$	$2.71 \cdot 10^3$	kg/m^3
$\boldsymbol{K_c}$	10^{10}	–
$\boldsymbol{\rho_{CaO}}$	$3.35 \cdot 10^3$	kg/m^3
$\boldsymbol{\|\Delta H\|}$	200	kJ/mol
$\boldsymbol{\mu_f}$	10^{-4}	Pas
$\boldsymbol{\Delta E}$	197	kJ/mol

The Gruntfest number of this system expresses the ratio of a characteristic time scale of heat production over a characteristic time scale of energy transfer, i.e. heat absorbed/released due to chemical reactions. In this work we have two volumetric heat loss mechanisms that absorb the produced heat due to friction, namely endothermic chemical reactions and heat diffusion. The limits of the Gruntfest number provide insights for the physical processes that characterize each regime. Indeed, when $Gr \to 0$ or $\beta_T \tau_n \dot{\gamma}_0 \ll k_F |\Delta H| \rho_{AB}$, the heat produced due to friction is significantly smaller than the one that the system can absorb until the reaction is triggered. Therefore at this limit of low Gruntfest numbers the only "active" mechanism is friction. On the other hand, when $Gr \to \infty$ or $\beta_T \tau_n \dot{\gamma}_0 \gg k_F |\Delta H| \rho_{AB}$, the heat produced due to friction is significantly larger than the one that the system can absorb until the reaction is triggered. In such a state, the system has enough energy to set the reaction in, leading to the assumption that at this limit of high Gruntfest numbers the behavior is mainly determined by the nature of the chemical reaction. Since the critical parameter that may vary with strain rate, temperature and pressure is the Taylor-Quinney coefficient β_T, the Gruntfest number is in principle not constant and hence it is chosen as a bifurcating parameter.

The dimensionless parameter Le is called the Lewis number and expresses the ability of the system to diffuse heat over the ability of the system to diffuse mass. In a recent work Veveakis et al. (2010) considered it constant, and under the assumption of condensed matter (i.e. that all the reactants and products are either in solid or liquid state), it was required that $Le \gg 1$. However, in this study, where we specify the chemical reaction and its influence in the porous medium, Le is in principle varying with temperature and pore pressure, following the porosity variations through Eq. (6). In the pertinent literature, the permeability of a fault is strongly varying, admitting values between 10^{-21}– $10^{-15} m^2$ and is reported (Rice 2006, Sulem and Famin 2009) to strongly affect the stability and evolution of faults in the pressurization regime. Thus Le is between $10^{-3} - 10^{3}$, being maximum at low permeabilities. This fact, along with the need for a more realistic permeability model in the presence of chemical reactions leads us to further study the effect of this parameter to the stability of the system.

The expression Ar is the Arrhenius number which measures the magnitude of the activation energy of the reaction, and determines the spectrum of the temperature field that the chemical reaction takes place (Law 2006, p. 59-62). As a consequence, this number is reaction-dependent and should be evaluated through measurements at the conditions of the problem at hand. For the reaction of calcite decomposition $E_F = 200\, kJ/mol$ at around $600℃$ (Sulem and Famin 2009). Thus, the corresponding Arrhenius number is considered here to be around 40.

Following the definition of $Ar_d = (x/N)Ar$, the ratio a could be understood as the relative difference of the Arrhenius numbers of the two reactions ($a = (Ar - Ar_d)/Ar$). It expresses the relative difference of the energy thresholds the two reactions set in and admitting values in the range $0 < a < 1$, since rate and state sensitivity is expected to precede always the onset of the chemical reaction Veveakis et al. (2010). At the limit $a \to 1$, or $Ar_d \to 0$, friction requires negligible energy to start producing heat. On the other extreme, when $a \to 0$, or $Ar_d \to Ar$, friction requires energy comparably close to the activation energy of the reaction. Veveakis et al. (2010) have estimated a from the experiments of Leinenkugel (1976) in kaolinite and the values of the activation energy E, x to be $a \sim 0.1$. In order to provide better estimates of this parameter, we need to

identify the various mechanisms taking place at the microscale and determine the rate and state dependency of friction. Nonetheless, as shown in Fig. 7 of Veveakis et al. (2010), the stability regimes of the system depend on both the boundary temperature and a, and there is always a maximum value of T_b below which the same qualitative results could be obtained. This means that we could choose a constant value for a (here 0.5) and vary temperature at the boundary to provide similar behavior.

The ratio δ incorporates the two volumetric heat loss mechanisms of the problem. Taking into account the fact that usually $\sim E_F$, and thus the specific enthalpy is comparable to the value of the activation energy, $\Delta H \approx E_F$, we may rewrite it for calcite decomposition as $\delta = R\left(\rho_{CaCO_3}/k_m\right)(d/2)^2 k_F Are^{-Ar}$. By using indicative values from Table 1, we can obtain for δ and for the reaction rate coefficient μ_r

$$\delta \approx 10^{-2} Ar \cdot k_F\, e^{-Ar}, \mu_r \approx k_F e^{-Ar} \tag{19}$$

These expressions depict that the two numbers may vary significantly, since Ar and k_F may admit values from a broad range. However, we notice that $\delta \approx \mu_r$ always, and that for $Ar = 40$ and $k_F = 10^{15} s^{-1}$, we can approximate $\delta \approx \mu_r \sim 10^{-3}$.

As becomes apparent from the equations and this analysis, the system is driven mainly by Gr in the heat equation and Le in the pore-pressure one. The role of each of these numbers on the response of the system during creep deformation will be highlighted in the following sections by performing a numerical bifurcation.

4. STEADY STATE CREEP

4.1 Numerical results

Since the transient system of Eqs. (16) is valid in the vicinity of its steady state, its behavior could be understood by resorting to the corresponding steady state system of equations,

$$\begin{aligned} \frac{1}{Le}\frac{\partial^2 \Delta p}{\partial z^2} + \zeta \mu_r e^{\frac{Ar\delta T}{1+\delta T}} &= 0 \\ \frac{\partial^2 T}{\partial z^2} + \left[Gr(1-\Delta p)^{-1/N} e^{\frac{\alpha Ar}{1+\delta T}} - 1\right] e^{\frac{Ar\delta T}{1+\delta T}} &= 0 \end{aligned} \tag{20}$$

The stability analysis of Eqs. (16) is performed by means of an arc-length continuation method (Chan and Keller 1991) for the steady-state problem of Eqs. (20) in order to calculate the system's solutions with respect to Gr as a bifurcating parameter. The system is solved with drained, isothermal boundary conditions and for the values of the dimensionless group appearing in Table 1. In Fig. 2 (a) and (b) we present the variation of the core temperature and the excess pore pressure with Gr comparing the typical system response for VHTS and VSTH. The results verify the information obtained from the asymptotic analysis, since the system depicts two distinct behaviors due to excess pore-pressure generation, depending on the choice of the friction law.

Despite of the difference in the higher temperature regime, it is worth noticing that the two bifurcation diagrams are identical in the lower temperature one, as a result of

the very low increase of Δp up to the second turning point. This is in agreement with Veveakis et al. (2010). Therefore, the pore pressure diffusion equation (Eq. 25 (a)) is inactive for low temperatures and for this specific set of parameters, as explained in the asymptotic analysis. This means that the lower temperature regime is mainly frictional and is strongly affected by the boundary temperature.

In Fig. 3 we present the variation of the core temperature and the excess pore pressure with Gr, for various values of the boundary temperature (in the VHTS case). As expected (from the works of Law 2006, Veveakis et al. 2010) increasing the boundary temperature would alter the response curve from a folded to a stretched one, eliminating the intermediate branch. It is also worth noticing that the existence of the system's higher temperature solutions are unaffected by T_b. We may therefore verify that, up to the second turning point, C, the only active mechanism is shear heating due to friction, and the pore pressure equation is inactive, as suggested by the pore pressure response depicted in Fig. 2(b). It is worth noticing that the upper branches (CD-DE) are insensitive to boundary temperature, implying that the system has admitted adiabatic conditions and is mainly driven by the hydrothermal response of the material, expressed through Le and Gr. In view of this result, and based on the results of Veveakis et al. (2010), we conclude that the upper branches are mainly influenced by the chemical reaction.

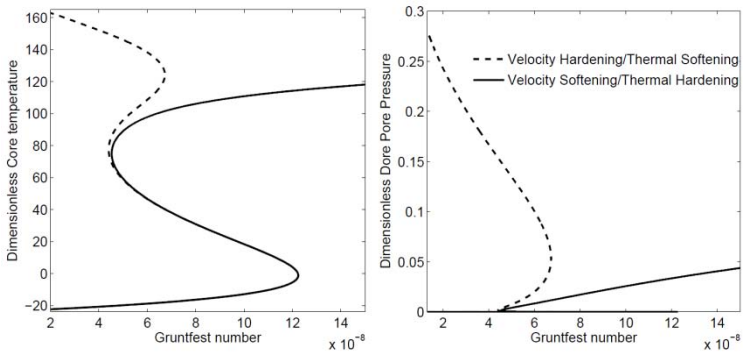

Fig. 2 Response curves for velocity hardening - thermal softening and vice versa of (a) the Dimensionless Core Temperature and (b) the Dimensionless Core Excess Pore-Pressure. The results are obtained for $Le = 0.01$.

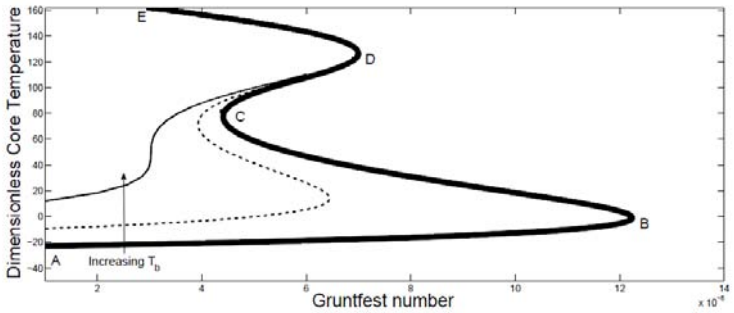

Fig. 3. System's response and impact of the boundary conditions: Response curves for varying boundary temperature.

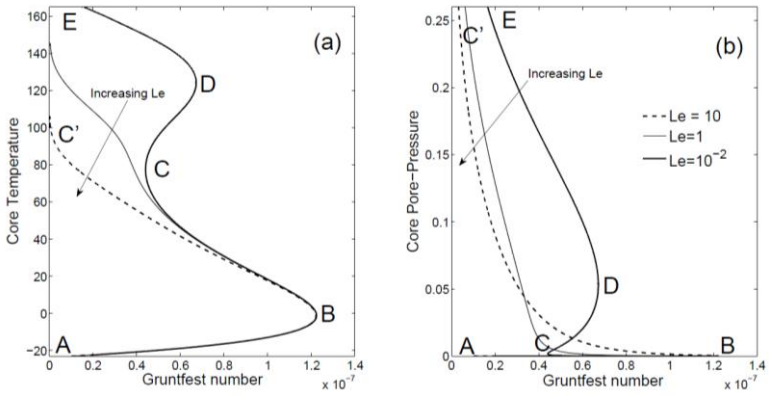

Fig. 4 Response curves for various values of Le in the VHTS case.

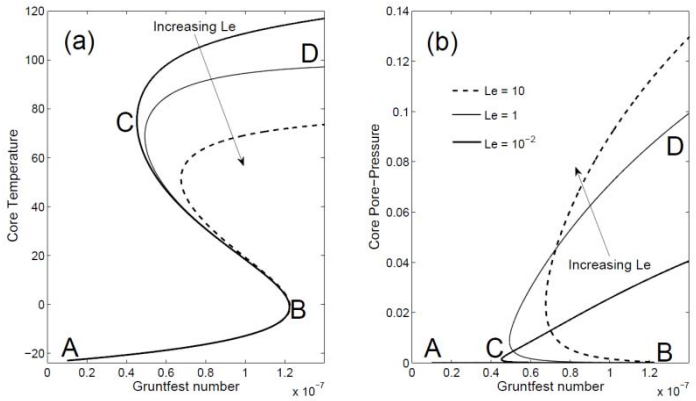

Fig. 5 Response curves for various values of Le in the VSTH case.

In Fig. 4 and 5 we present the response curves of the system for different values of the Lewis number in the VHTS and the VSTH case, respectively. We observe that, in analogy with the effect of T_b at the lower branches of the system, Le influences the behavior of the upper ones causing the loss of the intermediate (CD), as the upper (DE) branch merges with the second one (BC) in VHTS, while in the other case (VSTH) it lowers the upper (CD) branch implying that pressurization sets in at lower temperatures, as Le increases. The stability of these branches is discussed in the following.

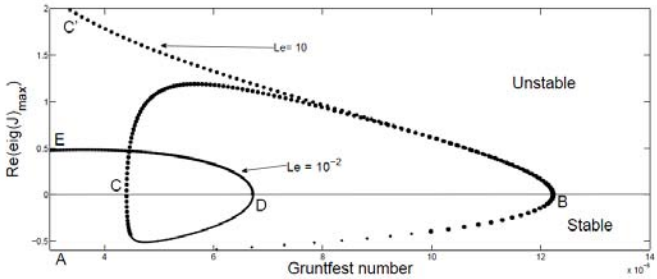

Fig. 6 Real part of the eigenvalues for velocity hardening and thermal softening

4.2 Steady state analysis (the VHTS case)

The stability of the steady-state branches appearing in the responce curve A-B-C-D-E of Fig. 4 could be determined by the eigenvalues of the numerical Jacobian matrix, since the appearance of positive real parts marks the onset of instability (Chan and Keller 1991). In Fig. 6, we present the maximum eigenvalues for low (Le = 0.01) and high (Le = 10) Lewis numbers, respectively. By noticing that the eigenvalues are always real in this case, we conclude that for the former case (Le = 0.01) the lower branch (AB) is stable followed by three branches of alternating stability (namely BC-unstable, CD-stable, DE-unstable). In the latter case (Le = 10), as already stated, there are only two steady state solutions, the curve of a Bratu-like problem (Chan and Keller 1991) is retrieved, where the stable lower branch AB is followed by an unstable one. In both cases, the upper branches correspond to excess pore-pressure increase due to the chemical reaction, as shown in Fig. 4(b).

From the physical point of view, the lower branch is a stable frictional one, on which the fault would creep stably with minimal chemical effects. It is followed by the unstable BC branch, where localization of deformation and dissipation takes place, as shown by Veveakis et al. (2010). In the third branch (CD), the chemical effects become strong enough to counterbalance the heat produced due to friction. Thus the fault may creep stably in this regime as well, in a higher energy state of elevated temperatures and excess pore pressures. Any fluctuations from this state would correspond to pore pressure increase bounded by the fourth branch in temperature and pore-pressure. Notably, since the upper branches appear only at low values of Le (i.e. high permeability), they signify that the porous medium is permeable enough to diffuse away a portion of the produced chemical overpressure and stabilize the system in a higher energy state. As permeability reduces, thus decreasing the diffusing capability of the fabric, the stable branch CD seizes to exist and the system becomes unstable at the onset of chemical pressurization.

Since the Gruntfest number is kept constant in the present setting, not allowing to the system to trace all the A-B-C-D-E curve, the stable branches (AB,CD) are acting as global attractors, whereas the unstable ones (BC,DE) as repellers. Due to the fact that the unstable upper branch (DE) is not bounded, if it is surpassed, an unbounded increase in temperature and pore pressure would occur, leading the system to fluidization. The same behavior will take place in the areas of Gr beyond point B (or D, depending on the values of Le and T_b), where no steady solution exists.

4.3 Steady state analysis (the VSTH case)

For a material exhibiting Velocity Softening – Thermal Hardening frictional behavior, the corresponding bifurcation diagrams (Fig. 5) reveal three steady-state solution branches forming a so-called folded S-curve, verifying the results of the asymptotic analysis. Notably, the decrease of the core temperature with increasingLe, leads to the assumption that if the latter admits a higher value, the two turning points could vanish and the curve would become a stretched one. This argument is corroborated in the following, revealing a rather complex behavior of the system with the Lewis number. Also, Fig. 5(b) verifies that for a specific Gruntfest number, the excess pore-pressure is larger the higher Le becomes.

Due to the aforementioned complexity of the system, we present the response diagrams with varying Le and boundary temperature, and indicate the stability of each solution branch on them (Fig. 7). As in the previous regime, the boundary temperature influences the two lower branches and for values high enough it results in stretched S-curves, similar to the ones obtained in Veveakis et al. (2010). The same result could be obtained for very large Lewis numbers, Fig. 7(10), given a boundary temperature. Nonetheless, we should always keep in mind that if T_b is reduced well below the geothermal value the system again admits a folded S-curve type response.

As shown in Fig. 7, the lower branch is stable (frictional regime), the intermediate one is unstable (localization regime) and the upper (chemical reaction regime) could be either stable, unstable or with changing stability. Indeed, upon reaching the upper branch, the real part of the maximum eigenvalue may change signs (Fig. 8(11)−(33)). The most important change however, with respect to the VHTS case, is that after the upper turning point the eigenvalues of the solutions become complex. This fact could be an indication for the onset of oscillatory instabilities at the upper branch, which is a quite common response of systems in the field of diffusion flames, where the same class of equations is studied (Hsuen and Sotirchos 1991). In geomechanics oscillatory instabilities are usually met in the spring-block models with rate and state dependent friction laws (Gu et al. 1984, Hahner and Drossinos 1998).

The main drawback of the present analysis is that we cannot extract conclusive results for the exact behavior of the system on the upper branch, since oscillatory instabilities are transient modes and could not be approached with a steady state analysis. In order to investigate the nature and impact of oscillatory instabilities, the time-dependent system of equations must be integrated numerically, scanning (i.e. varying the initial conditions) the phase diagram for limit cycles or spiral modes of instabilities.

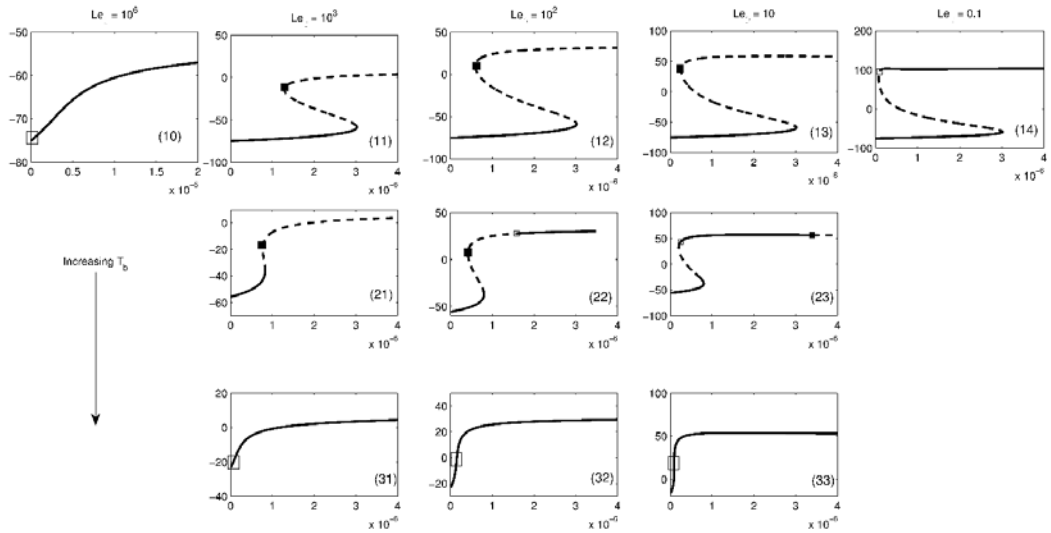

Fig. 7 Response diagrams (Gr vs T) for different T_b and Le. The branches plotted as solid curves are solutions having eigenvalues with negative real part (stable), whereas the dashed ones with positive real part (unstable). The rectangles depict the onset of complex eigenvalues; solid black for positive real part and empty for negative one.

5. TRANSIENT ANALYSIS OF THE VSTH CASE

From the steady state diagram, Fig. 8(a), we may recognize 3 areas of interest, depending on the value of Gr. These areas correspond to 1) low values of Gr, below the upper turning point C, 2) Intermediate Gr values, between points C and B, 3) High Gr values, above point B. The system is then integrated, for arbitrary values of Gr in each of those areas (in this case we choose $Gr = 10^{-7}, 10^{-5}, 3 \cdot 10^{-5}$ as indicated in Fig. 8(a) with the lines (I-II-II) respectively). The resulting phase diagrams (in the dimensionless $\Delta p - T$ space) of Figs. 8(b)-(d) may then be used to provide a physical explanation for the evolution of the system on each of these areas.

5.1 The area of stable, aseismic creep, line I

In this area the system has only one, stable, steady-state solution, namely the point $(\Delta p, T) = (0, -99.98)$, indicated with a circle on line (I), in Fig. 8(a). As verified by the results of Fig. 8(b), this point acts as a global attractor in the transient regime, i.e. irrespectively of the initial conditions imposed, the system will end up there. Therefore, in this area the fault is in state of stable, aseismic creep.

5.2 The area of non-periodic seismic events, line II

The behavior of the system in this area is not as straightforward as the previous one, having three steady state solutions. The upper equilibrium solution (indicated with a triangle) has complex eigenvalues, pertaining to the existence of oscillatory modes of instability. The phase plane analysis of Fig. 8(c) reveals that the aforementioned equilibrium solution acts as a spiral repeller. The lower (stable) steady state solution (depicted as a circle in Fig. 8(c)) acts as a global attractor, and the intermediate equilibrium solution (highlighted with a rectangle in Fig. 8(a)) is unstable. In this area, the phase diagram provides the line b-c as a separatrix. Above this separatrix the intermediate equilibrium solution repels the orbits towards the global attractor, through the spiral track induced by the upper spiral repeller. Any initial condition will force the system first to a shear heating phase, where temperature increases without pressure variations. This is followed by a fast pore pressure production phase, during which temperature drops and leads to the final relaxation phase -where temperature and pore pressure decrease- towards the global attractor. On the contrary, for initial conditions lying below the separatrix b-c the system evolves rapidly towards the global attractor.

We may further understand the behavior of the system by plotting (Fig. 9) the evolution of the strain rate (Eq. 12), for each of these two areas. As expected, in the area below the separatrix the strain rate goes directly into its slow, stable value, creeping stably with inappreciable rates (dashed line of Fig. 8). On the other hand, above the separatrix the evolution of the strain rate provides a fast acceleration phase, followed by a progressive decceleration towards the global attractor, where it relaxes creeping at low rates (solid line of Fig. 9). Since the acceleration (slope of the curve) increases rapidly and then obtains an almost constant, small value during relaxation, we may interpret this event as a single, non-periodic stress drop event for the overlying rigid block followed by a recovery period relaxing back to stable creep at inappreciable rates.

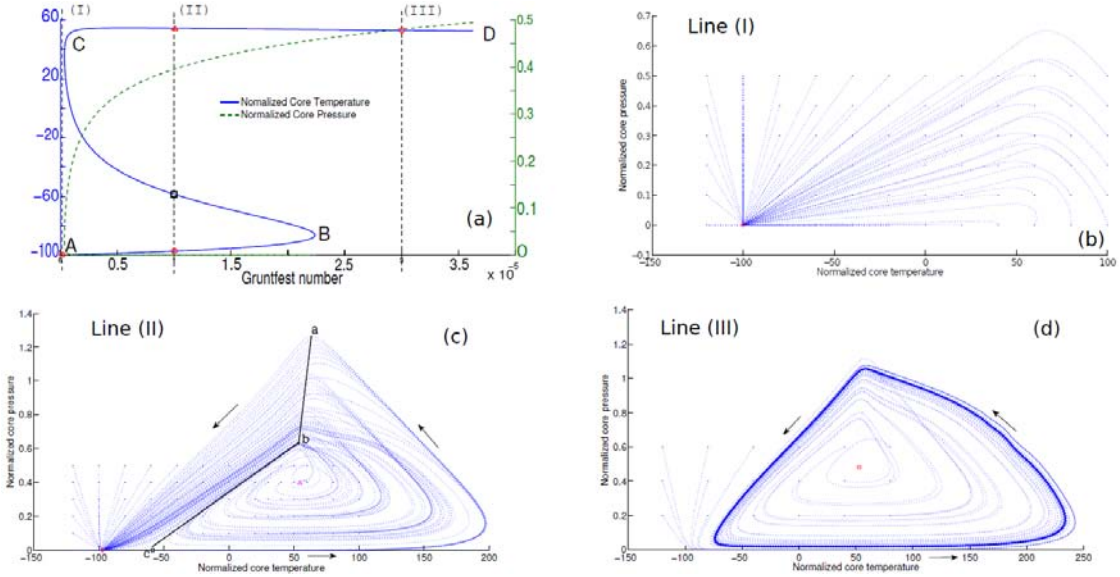

Fig. 8 Summary of the steady state and transient response for the parameters used ($Le = 1$, $T_b = 440$℃).

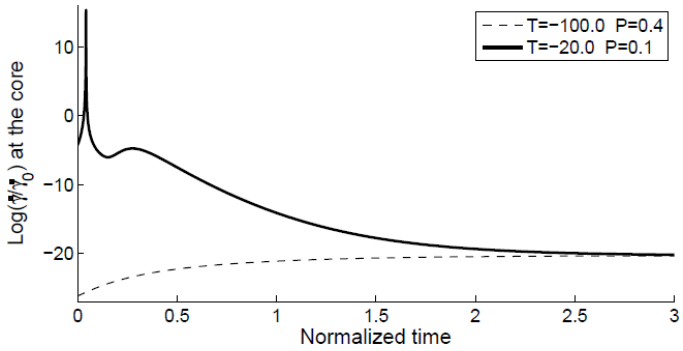

Fig. 9 Evolution of the core strain rate on line II of Fig. 8a, for an initial condition below (dashed line) and above (solid line) the unstable middle branch.

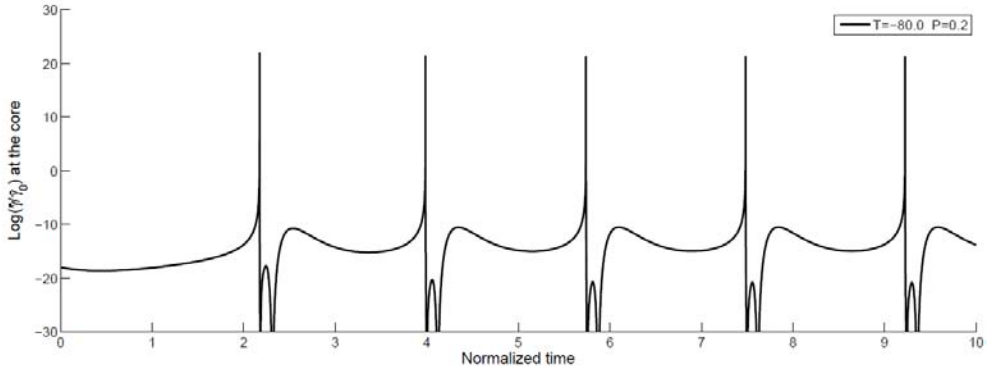

Fig. 10 Evolution of the core strain rate on line III of Fig. 4 (a).

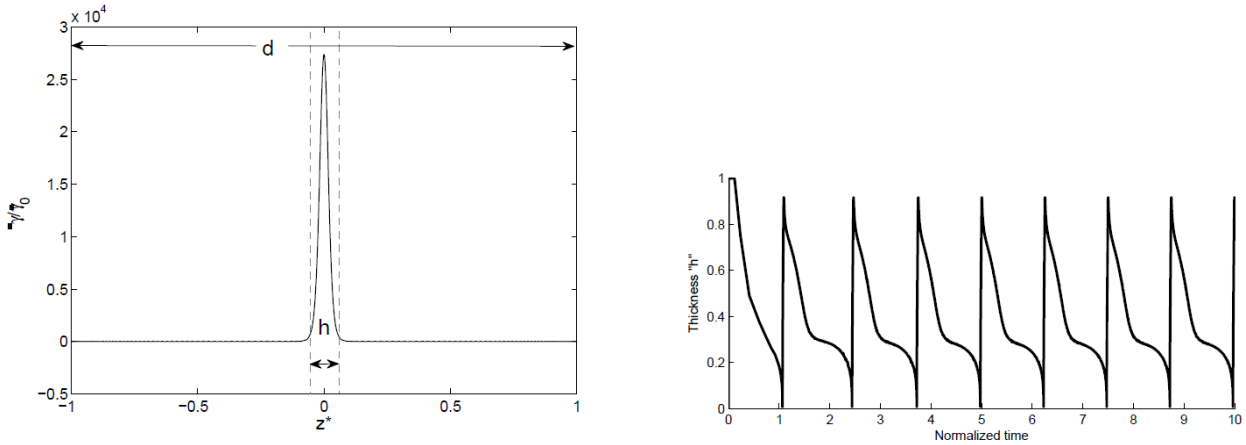

Fig. 11 (a) Profile of the strain-rate inside the shear zone. Notice the strain-rate localization, in a thin core h where chemical events take place. (b) Evolution of h.

5.3 The area of periodic events, line III

In this area, the single steady state solution is expected to be unstable and any limit cycles should be stable. Indeed, when the system is integrated for initial values along line III, Fig. 8(a), the orbits follow the cycle depicted in Fig. 8(d). Similarly to the previous case, any initial condition will force the system to an initial shear heating phase, increasing its temperature with constant pore pressure. Upon the triggering of the chemical reaction, pressurization sets in up to the maximum value of excess pore pressure. Then, the system starts relaxing, decreasing both temperature and pore pressure to their lower values (here -70 and 0.1 respectively), to repeat the cycle.

These results can be casted in a physically meaningful framework, when plotting the corresponding evolution of the strain rate (Fig. 10). We notice that in this area the strain rate undergoes periodic events of abrupt increase and smooth decrease. In fault mechanics terminology we would interpret this behavior as periodic stress drop-recovery events along the same fault. By plotting the profile of the strain rate inside the shear zone (Fig. 11(a)) we may notice that all the seismic events (i.e. spikes in the strain rate evolution) are taking place in an ultra-localized zone called principal slipping zone (PSZ) of the fault (Chester and Chester 1998, Rice 2006). The evolution of h verifies this claim, spanning from the whole shear zone to a PSZ two orders of magnitude narrower during the limit cycle (Fig. 11(b)) where chemical reaction sets in.

6. CONCLUSIONS

In this paper we presented a thermo-chemo-mechanical approach of the problem of a fluid saturated fault under shear. We have shown that by introducing a rate-and-state dependency on the friction coupled to the effect of a decomposition reaction that produces excess pore-fluid and reduces the strength of the fault, we may obtain qualitatively the behavior of a fault both at creeping and seismic regimes. We verify that the pressurization due to the fluid produced from the chemical reaction itself could be powerful enough to determine the dynamic weakening of faults. Such models may qualitatively reproduce the behavior of the well-known spring-block models and provide

limit cycles that correspond to stick-slip instabilities, as shown in Section 5. However, we emphasize the fact that instead of attributing these instabilities to the influence of an elastic rigid block that drives the system, in this case they are attributed to the presence of an endothermic chemical reaction that has the potential to absorb the heat produced due to friction and bring the system to lower temperatures, and thus excess-pore pressures.

The advantage of these multi-physical approaches lies on their capability to provide additional information towards the quantitative assessment of the behavior of faults. In addition, they are characterized by great multiplicity in their use. In this study we verified this claim showing that when an arbitrary chemical reaction is considered, the problem exhibits a rich multiplicity of stability structure. Given this fact and the capability of the model to calculate the timescales of the various processes, the presented formulation seems promising to provide convincing answers for the Mechanics and Physics of faults. However, in order to be able to calibrate such models, answers remain to be given on the exact mechanisms of friction in geomaterials, as well as the actual reaction rates of the chemical processes at seismic depths. The model neglects also the fault's geometry (as a propagating shear band). Hence, constitutive fabric effects should be taken into consideration, as they are expected to differentiate the strain accumulation and the soil strength at various locations along the fault.

ACKNOWLEDGEMENT

The research leading to these results has received funding from the European Research Council under the European Union's Seventh Framework Program (FP7/2007-2013) / ERC IDEAS Grant Agreement n° 290963 (SOMEF).

REFERENCES

Brantut, N., Schubnel, Rouzaud, J., Brunet, F. and Shimamoto., T. (2008), "High velocity frictional properties of a clay-bearing fault gouge and implications for earthquake mechanics", *J. Geophys Res.*, Vol. **113**, B10401.

Brantut, N., Schubnel, A., Corvisier, J. and Sarout, J. (2010), "Thermochemical pressurization of faults during coseismic slip", *J. Geophys Res.*, Vol. **115**, B05314.

Chan, T. and Keller, H. (1991), "Arc-length continuation and multi-grid techniques for nonlinear elliptic eigenvalue problems", *SIAM J. Sci. Stat. Comp.*, Vol **3**(2), 173–194.

Chen, H., Douglas, A.S. and Malek-Madani., R. (1989), "An asymptotic stability condition for inhomogeneous simple shear", *Q. Appl. Math.*, Vol. **47**, 247–262.

Chester, F.M. and Chester, J.S. (1998), "Ultracataclasite structure and friction processes of the punchbowl fault, San Andreas system, California", *Tectonophysics*, Vol. **295**, 199–221.

Dieterich, J. (1972), "Time-dependent friction in rocks", *J. Geophys. Res.*, Vol. **377**, 3690–3697.

Dieterich, J. (1978), "Time-dependent friction and the mechanics of stickslip", *Pure Appl. Geophys.*, Vol. **116**, 790–806.

Ferri, F., Toro, G. D., Hirose, T. and Shimamoto, T. (2010) "Evidence of thermal pressurization in high-velocity friction experiments on smectiterich gouges", *Terra Nova*, doi:10.1111/j.1365–3121.2010.00955.x.

Fialko, Y. and Khazan, Y. (2005), “Fusion by earthquake fault friction: Stick or slip?”, *J. Geophys. Res.*, Vol. **110**, B12407.
Gu, J., Rice, J.R., Ruina, A.L. and Tse, S.T. (1984), “Slip motion and stability of a single degree of freedom elastic system with rate and state dependent friction”, *J. Mech. Phys. Solids*, Vol. **32**(3), 167–196.
Hahner, P. and Drossinos, Y. (1998), “Nonlinear dynamics of a continuous springblock model of earthquake faults”, *J. Phys. A: Math. Gen.*, Vol. **31**, 185–191.
Han, R., Shimamoto, T., Hirose, T., Ree, J. and Ando, J. (2007), “Ultralow friction of carbonate faults caused by thermal decomposition”, *Science*, Vol. **316**, 878–881.
Hirono, T., et al. (2007) “A chemical kinetic approach to estimate dynamic shear stress during the 1999 Taiwan Chi-Chi earthquake”, *Geophys. Res. Lett.*, Vol. **34**, L19308, doi:10.1029/2007GL030743.
Hsuen, H. and Sotirchos, S. (1991) “Multiplicity and stability phenomena in diffusion flames”, *Chemical Engineering Science*, Vol. **12**, 3165–3175.
Law, C. (2006), *Combustion Physics*, Cambridge University Press.
Leinenkugel, H. (1976), “Deformations und festigkeitverhalten bindiger erdstoffe: Experimental ergebnisse und ihre physikalische deutung”, doctoral Dissertation, Univ. Karlsruhe, Karlsruhe, Germany
Rice, J.R. (2006), “Heating and weakening of faults during earthquake slip”, *J. Geophys. Res.*, Vol. **111**, B05311.
Rognon, P. and Einav, I. (2010), “Thermal transients and convective particle motion in dense granular materials”, *Phys. Rev. Letters*, Vol. **105**, 218–301.
Ruina, A. (1983), “Slip instability and state variable friction laws”, *J. Geophys. Res.*, Vol. **88**(B12), 10359–10370, doi:10.1029/JB088iB12p10359.
Sulem, J. and Famin, V. (2009), “Thermal decomposition of carbonates in fault zones: slip-weakening and temperature-limiting effects”, *J. Geophys. Res.*, Vol. **114**, B03309.
Sulem, J., Lazar, P. and Vardoulakis, I. (2007), “Thermo-poro-mechanical properties of clayey gouge and application to rapid fault shearing”, *Int. J. Num. Anal. Meth. Geomechanics*, Vol. **31**(3), 523–540.
Vardoulakis, I. (2002), “Dynamic thermo-poro-mechanical analysis of catastrophic landslides”, *Geotechnique*, Vol. **52**, 157–171.
Vardoulakis, I. and Sulem, J. (1995), *Bifurcation Analysis in Geomechanics*, Blankie Acc. and Professional.
Veveakis, E., Alevizos, S. and Vardoulakis., I. (2010), “Chemical reaction capping of thermal instabilities during shear of frictional faults”, *J. Mech. Phys. Sol.,* Vol. **58**, 1175–1194.
Veveakis, E., Sulem, J. and Stefanou, I. (2012), “Modeling of fault gouges with cosserat continuum mechanics: Influence of thermal pressurization and chemical decomposition as coseismic weakening mechanisms”, *J. Struct. Geology*, in press.
Veveakis, E., Vardoulakis, I. and Toro., G.D. (2007), “Thermoporomechanics of creeping landslides: The 1963 vaiont slide, northern Italy”, *J. Geophys. Res.*, Vol. **112**, F03026.
Yund, R., Blanpied, M., Tullis, T. and Weeks, J. (1990), “Amorphous material in high strain experimental fault gouges”, *J. Geophys. Res.*, Vol. **95**(B10), 589–602.